

# A Robin-Neumann Scheme with Quasi-Newton Acceleration for Partitioned Fluid-Structure Interaction

Thomas Spenke\*, Michel Make, Norbert Hosters

Chair for Computational Analysis of Technical Systems (CATS),  
 Center for Simulation and Data Science (JARA-CSD),  
 RWTH Aachen University,  
 Schinkelstraße 2, Aachen, Germany

---

## Abstract

The Dirichlet-Neumann scheme is the most common partitioned algorithm for fluid-structure interaction (FSI) and offers high flexibility concerning the solvers employed for the two subproblems. Nevertheless, it is not without shortcomings: To begin with, the inherent added-mass effect often destabilizes the numerical solution severely. Moreover, the Dirichlet-Neumann scheme cannot be applied to FSI problems in which an incompressible fluid is fully enclosed by Dirichlet boundaries, as it is incapable of satisfying the volume constraint.

In the last decade, interface quasi-Newton methods have proven to control the added-mass effect and substantially speed up convergence by adding a Newton-like update step to the Dirichlet-Neumann coupling. They are, however, without effect on the incompressibility dilemma. As an alternative, the Robin-Neumann scheme generalizes the fluid's boundary condition to a Robin condition by including the Cauchy stresses. While this modification in fact successfully tackles both drawbacks of the Dirichlet-Neumann approach, the price to be paid is a strong dependency on the Robin weighting parameter, with very limited a priori knowledge about good choices.

This work proposes a strategy to merge these two ideas and benefit from their combined strengths. The effectiveness of this new quasi-Newton-accelerated Robin-Neumann scheme is demonstrated for different FSI simulations and compared to both Robin- and Dirichlet-Neumann variants.

**Keywords:** Partitioned Fluid-Structure Interaction, Robin-Neumann Scheme, Interface Quasi-Newton Methods

---

## 1. Introduction

Partitioned solution schemes for multi-physics problems are widely used in modern computational mechanics due to their modularity: Treated as black boxes, the distinct solvers employed for the subproblems are coupled only via the exchange of interface data. In fluid-structure interaction, the prevalent partitioned algorithm is the *Dirichlet-Neumann (DN)* scheme, which passes the fluid loads at the interface as a Neumann condition to the structural solver, before the resulting deformation state imposes a Dirichlet condition on the flow problem.

Despite its popularity, the Dirichlet-Neumann scheme comes with two significant drawbacks addressed in this work: (1) Its pronounced sensitivity to the *added-mass effect* not uncommonly causes the coupling iteration to diverge, preventing any numerical solution [1–4]. (2) It fails to work for FSI simulations with a fully-enclosed incompressible fluid, i.e., if the velocity field is prescribed by Dirichlet conditions on all boundaries, such as for example the inflation of a water balloon. Because in that case, the fluid volume is uniquely defined by the structural deformation, which does not account for the flow's incompressibility, causing what is referred to as the *incompressibility dilemma* [5, 6].

---

\*Corresponding author

Email addresses: [spenke@cats.rwth-aachen.de](mailto:spenke@cats.rwth-aachen.de) (Thomas Spenke), [make@cats.rwth-aachen.de](mailto:make@cats.rwth-aachen.de) (Michel Make), [hosters@cats.rwth-aachen.de](mailto:hosters@cats.rwth-aachen.de) (Norbert Hosters)

When it comes to tackling the added-mass instability, *interface quasi-Newton (IQN)* methods have been a vibrant field of research in recent years, as they both stabilize and accelerate partitioned schemes [7–9]. Identifying the converged time step solution as a fixed point of the coupling loop, their key idea is to add a Newton-like update step of the exchanged data fields, e.g., the interface deformation. As the inverse Jacobian required for Newton’s method is typically inaccessible, it is approximated instead.

After first pioneer works in the field [10, 11], the interface quasi-Newton *inverse least-squares (ILS)* method by Degroote et al. [12] marked an important milestone, as it introduced the least-squares approximation of the inverse Jacobian that has become standard today. Initially, it relied only on input-output data pairs collected within the current time step. Follow-up research revealed, however, that using past time step data is very advantageous, but also challenging: An explicit reutilization of data pairs may suffer from rank deficiency and the dependency on the number of reused time steps – although both effects can be alleviated by proper filtering techniques [13, 14]. An implicit incorporation via an updated Jacobian, on the other hand, avoids these issues, but typically brings along a costly explicit Jacobian [8, 9]. However, recent formulations circumventing this drawback were presented by Scheufele and Mehl [15] as well as Spenke et al. [16]. Aside from reusing past time step data, an interesting and rather new strategy is to enhance the Jacobian approximation with a surrogate model, obtained for example from simplified physics or coarser discretizations [17, 18].

While update steps of the interface data, like quasi-Newton methods, can overcome the added-mass instability, they are without effect on the incompressibility dilemma, as it is inherent to the Dirichlet-Neumann communication pattern itself. One countermeasure is therefore to change this very pattern. In 2008, Badia et al. [19] as well as Nobile and Vergara [20] first proposed the usage of Robin-based schemes: Rather than transferring either Dirichlet or Neumann interface data, these approaches make use of Robin conditions to linearly combine the two contributions. Bearing in mind the special cases of either contribution being zero, the Dirichlet-Neumann scheme can in fact be sorted into the more general family of Robin-Robin schemes.

In this work, however, another member is of particular interest, the *Robin-Neumann (RN)* scheme: While the fluid tractions are passed to the structural solver just as in the Dirichlet-Neumann case, both the structure’s deformation and tractions are returned to the fluid problem, forming a Robin boundary condition. It can be pictured as adding some numerical permeability to the FSI interface, allowing for artificial fluid fluxes that vanish when convergence is reached. The capability of temporarily violating kinematic continuity not only counteracts the added-mass effect, but also frees the Robin-Neumann scheme from the incompressibility dilemma, as fully-enclosed cases no longer have Dirichlet boundaries only. Unfortunately, however, the Robin-Neumann scheme also introduces new drawbacks. In particular, its performance is strongly governed by the Robin parameter that controls the weighting of Dirichlet and Neumann contributions; and although tuning this parameter has been studied for various simplified FSI problems [21–24], efficient choices are in general problem-dependent and difficult to find a priori.

As pointed out by Degroote [25], Robin-based schemes bear some analogy to artificial compressibility methods [6, 26], which weaken the incompressibility constraint to ensure kinematic continuity is satisfied rather than vice versa.

Both interface quasi-Newton methods and the Robin-Neumann scheme are preferable to the plain Dirichlet-Neumann approach in certain, slightly different aspects; but to the best of the authors’ knowledge, the two approaches have never been combined. Consequently, this work proposes a novel Robin-Neumann scheme with quasi-Newton acceleration that merges the strengths of both approaches. In particular, it provides a straightforward way of benefiting from the effectiveness of IQN methods for FSI simulations with fully-enclosed incompressible fluids, for which the Dirichlet-Neumann scheme is inapplicable. Beyond that, its potential performance gain over the Dirichlet-Neumann scheme for non-enclosed cases is investigated.

This work is outlined as follows: Section 2 presents the governing equations of the considered FSI problems, before Section 3 focuses on partitioned algorithms for fluid-structure interaction, including interface quasi-Newton methods and the Robin-Neumann coupling. Based on that, the new *Robin-Neumann quasi-Newton (RN-QN)* scheme is proposed in Section 4. Its performance is demonstrated in Section 5 via numerical test cases, covering both fully-enclosed and open fluid-structure interaction problems.

## 2. Problem Statement

In fluid-structure interaction, a fluid domain  $\Omega_t^f \subset \mathbb{R}^{n_{sd}}$  and a structural body  $\Omega_t^s \subset \mathbb{R}^{n_{sd}}$  share a boundary  $\Gamma_t^{fs} = \partial\Omega_t^f \cap \partial\Omega_t^s$ . The subscript  $t$  indicates the time level, while  $n_{sd}$  is the number of spatial dimensions. This section briefly presents the two subproblems, their numerical solution, and the coupling conditions arising at the interface  $\Gamma_t^{fs}$ .

### 2.1. Fluid Problem

The flow problem is governed by the unsteady *Navier-Stokes equations* for an incompressible fluid,

$$\rho_f \left( \frac{\partial \mathbf{u}_f}{\partial t} + \mathbf{u}_f \cdot \nabla \mathbf{u}_f - \mathbf{f}_f \right) - \nabla \cdot \mathbf{T}_f = \mathbf{0} \quad \text{in } \Omega_t^f \quad \forall t \geq 0, \quad (1a)$$

$$\nabla \cdot \mathbf{u}_f = 0 \quad \text{in } \Omega_t^f \quad \forall t \geq 0, \quad (1b)$$

that are solved for the fluid velocity  $\mathbf{u}_f(\mathbf{x}, t)$  and the pressure  $p_f(\mathbf{x}, t)$ . Therein,  $\rho_f$  is the constant fluid density, while  $\mathbf{f}_f$  denotes the resultant of all body forces per unit mass of fluid. Assuming a Newtonian fluid with dynamic viscosity  $\mu_f$ , the Cauchy stress tensor  $\mathbf{T}_f$  follows Stokes' law:  $\mathbf{T}_f(\mathbf{u}_f, p_f) = -p_f \mathbf{I} + \mu_f (\nabla \mathbf{u}_f + (\nabla \mathbf{u}_f)^T)$ , with the unit matrix  $\mathbf{I}$ .

The problem is closed by setting an initial flow field  $\mathbf{u}_f(\mathbf{x}, t = 0)$  and the following boundary conditions on the Dirichlet boundary  $\Gamma_{D,t}^f$ , the Neumann part  $\Gamma_{N,t}^f$ , and a Robin section  $\Gamma_{R,t}^f$ , with  $\Gamma_{D,t}^f \cap \Gamma_{N,t}^f \cap \Gamma_{R,t}^f = \partial\Omega_t^f$ :

$$\mathbf{u}_f = \mathbf{g}_f \quad \text{on } \Gamma_{D,t}^f \quad \forall t \geq 0, \quad (2a)$$

$$\mathbf{T}_f \mathbf{n}_f = \mathbf{h}_f \quad \text{on } \Gamma_{N,t}^f \quad \forall t \geq 0, \quad (2b)$$

$$\alpha^{RN} \mathbf{u}_f + \mathbf{T}_f \mathbf{n}_f = \mathbf{h}_f + \alpha^{RN} \mathbf{g}_f \quad \text{on } \Gamma_{R,t}^f \quad \forall t \geq 0, \quad (2c)$$

with the prescribed velocity  $\mathbf{g}_f$  and tractions  $\mathbf{h}_f$  [27]. Note that the Robin condition with its weighting factor  $\alpha^{RN}$  will contribute to both left- and right-hand side of the discrete system due to the unknown  $\mathbf{u}_f$ .

The fluid problem is solved by our in-house solver XNS, using P1P1 finite elements with *Galerkin/Least-Squares (GLS) stabilization* in space [28, 29] and a BDF1 scheme in time [30]. The ALE mesh is adapted to the deforming domain via the *linear elastic mesh-update method (EMUM)* [31, 32]; its velocity is determined using a first-order finite difference scheme, in line with the BDF1 integration of the flow problem [33].

### 2.2. Structural Problem

The structural displacement field  $\mathbf{d}_s(\mathbf{x}, t)$  is computed from the dynamic balance of inner and outer stresses. Using a total Lagrangian viewpoint, it is formulated in the undeformed configuration, indicated for all affected quantities by the subscript 0, such as  $\Omega_0^s$  or  $\nabla_0$ . The resulting equation of motion reads

$$\rho_s \frac{d^2 \mathbf{d}_s}{dt^2} = \nabla_0 \cdot (\mathbf{S} \mathbf{F}^T) + \mathbf{b}_s \quad \text{in } \Omega_0^s \quad \forall t \geq 0, \quad (3)$$

where  $\rho_s$  denotes the material density and  $\mathbf{b}_s$  the resultant of all body forces per unit volume. The deformation gradient  $\mathbf{F}$  relates the 2nd Piola-Kirchhoff stresses  $\mathbf{S}$  to the Cauchy stress tensor  $\mathbf{T}_s$ , with  $\mathbf{S} = \det(\mathbf{F}) \mathbf{F}^{-1} \mathbf{T}_s \mathbf{F}^{-T}$ . As constitutive equation, the St. Venant-Kirchoff material model provides the linear stress-strain law  $\mathbf{S}_s = \lambda_s \text{tr}(\mathbf{E}) + 2\mu_s \mathbf{E}$ , with the Lamé constants  $\lambda_s, \mu_s$  and the Green-Lagrange strains  $\mathbf{E} := \frac{1}{2} (\mathbf{F}^T \mathbf{F} - \mathbf{I})$  [34].

Aside from an initial deformation  $\mathbf{d}_s(\mathbf{x}, t = 0)$ , Dirichlet and Neumann conditions are defined to close the problem. They set the displacements  $\mathbf{g}_s$  on  $\Gamma_{D,0}^s \subset \partial\Omega_0^s$  and the tractions  $\mathbf{h}_s$  on  $\Gamma_{N,0}^s \subset \partial\Omega_0^s$ , with the outer unit normal  $\mathbf{n}_{s,0}$ :

$$\mathbf{d}_s = \mathbf{g}_s \quad \text{on } \Gamma_{D,0}^s \quad \forall t \geq 0, \quad (4a)$$

$$\mathbf{F} \mathbf{S} \mathbf{n}_{s,0} = \mathbf{h}_s \quad \text{on } \Gamma_{N,0}^s \quad \forall t \geq 0. \quad (4b)$$

The structural subproblem is numerically solved by the in-house finite-element code FEAFA using *isogeometric analysis (IGA)* [35, 36] in space and a *generalized- $\alpha$*  scheme in time [37, 38].

### 2.3. Coupling Conditions

It is the very essence of multi-physics simulations that the subproblems cannot be solved independently. For fluid-structure interaction, the solution fields are connected at the FSI interface  $\Gamma_t^{fs}$  via the following coupling conditions:

- The *kinematic* condition states the continuity of displacements,

$$\mathbf{d}_f = \mathbf{d}_s \quad \text{on } \Gamma_t^{fs} \quad \forall t \geq 0, \quad (5)$$

which analogously implies the equality of velocities  $\mathbf{u}_f = \mathbf{u}_s$  and accelerations  $\mathbf{a}_f = \mathbf{a}_s$ , too.

- In keeping with Newton's third law, the *dynamic* coupling condition requires the equality of interface tractions:

$$\mathbf{T}_f \mathbf{n}_f = \mathbf{T}_s \mathbf{n}_s \quad \text{on } \Gamma_t^{fs} \quad \forall t \geq 0. \quad (6)$$

Therein,  $\mathbf{n}_f$  and  $\mathbf{n}_s$  denote the associated unit normal vectors (with  $\mathbf{n}_f = -\mathbf{n}_s$ ).

If thermal effects are neglected, satisfying these coupling conditions for every time  $t$  in a continuous manner ensures the conservation of mass, momentum, and mechanical energy over the FSI boundary [5, 39].

## 3. Partitioned Fluid-Structure Interaction

Following a partitioned FSI coupling approach, the two subproblems, i.e., fluid and structure, are addressed by two distinct solvers, that are connected only via the exchange of interface data. While this strategy features a high flexibility and modularity regarding the two solvers, their communication requires some additional considerations:

- In general, the spatial discretizations do not match at the FSI boundary, so that the transfer of interface data requires a conservative projection. In this work, we employ a spline-based variant of the *finite interpolation elements (FIE)* method, see Hosters et al. [27, 40] and Make [39]. For the sake of simplicity, however, this *spatial coupling* will be neglected in the following as it does not interfere with the methods discussed.
- The interdependency between the two subproblems in general requires an iterative procedure to find a consistent solution of the coupled problem. This is referred to as *strong (temporal) coupling* [13, 27, 39].

### 3.1. Dirichlet-Neumann Scheme

The most widespread strongly-coupled algorithm for FSI problems is the *Dirichlet-Neumann (DN)* scheme. Its name stems from using the dynamic coupling condition to pass the fluid tractions as a *Neumann* boundary condition to the structure, before returning the resulting interface deformation – in accordance with kinematic continuity – as a *Dirichlet* condition to the fluid field<sup>1</sup>. The procedure is illustrated in Figure 1.

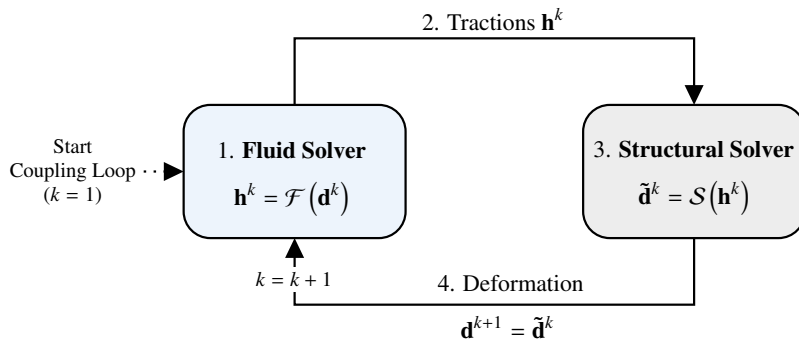


Figure 1: The coupling loop of the Dirichlet-Neumann scheme, iterated until convergence for every time step.

To simplify notation, the subscripts  $s$  and  $f$  of the interface deformation  $\mathbf{d}$  and the fluid tractions  $\mathbf{h}$ , respectively, are dropped henceforth. In every coupling iteration  $k$ , the following steps are repeated until convergence is reached:

<sup>1</sup>The Dirichlet condition of the fluid problem requires a velocity rather than a displacement. In this work, the mesh is first adjusted to the interface deformation, before the fluid motion is set to the resulting mesh velocity.

1. The fluid solver determines the tractions  $\mathbf{h}^k = \mathcal{F}(\mathbf{d}^k)$  based on the current deformation  $\mathbf{d}^k$ .
2. The tractions  $\mathbf{h}^k$  are passed to the structural solver,
3. which computes the resulting interface deformation  $\tilde{\mathbf{d}}^k = \mathcal{S}(\mathbf{h}^k)$ .
4. The deformation  $\tilde{\mathbf{d}}^k$  is sent to the flow solver and will be its input in the next iteration<sup>2</sup> i.e.,  $\mathbf{d}^{k+1} = \tilde{\mathbf{d}}^k$ .

The time step is considered converged if and only if the following two criteria are fulfilled:

- (I) Interpreting the coupling loop as a fixed-point iteration [7, 41], both subproblem solutions have to stay virtually unchanged within one coupling iteration, i.e., their relative changes have to be lower than some bound  $\varepsilon_{\text{Coupling}}$ .
- (II) For accurate results, the residuals of the two nonlinear subproblems have to satisfy their own convergence criterion  $\varepsilon_{\text{Problem}}$  before going on to the next time step.

Note that iterating both solvers to convergence in every call inherently fulfills the second condition, but typically causes a significant overhead in computation time. Therefore, this work uses the *N1-CC* strategy proposed in Spenke et al. [42], that is running only one Newton iteration per solver call, unless convergence criterion (I) is already met.

### 3.2. Added-Mass Instability and Incompressibility Dilemma

Being a partitioned algorithm, the Dirichlet-Neumann scheme suffers from the artificial *added-mass effect*: Due to calling the solvers in a staggered manner, in some coupling iteration(s) the subproblem solutions are inevitably computed with boundary conditions at  $\Gamma_t^{fs}$  that differ from the converged state still to be found. For instance, the flow field is generally updated based on an inexact interface deformation. In case this deformation is overestimated, kinematic continuity causes an exaggerated fluid acceleration at the interface, resulting in excessive inertia terms that act as an additional artificial fluid mass on the structure. This added-mass instability is in particular increasing with the density ratio between the fluid and the structure  $\rho_f/\rho_s$ , but the viscous terms and the time discretization are influencing factors as well. For more information on the added-mass effect, we recommend the works by Causin et al. [1], Förster et al. [2, 3], and van Brummelen [4].

Aside from the added-mass instability, the Dirichlet-Neumann scheme has a second weakness, referred to as *incompressibility dilemma*: It does not work for FSI problems in which an incompressible fluid is fully enclosed by Dirichlet conditions for the velocity, such as walls or prescribed inflows. For such a problem, the fluid volume is uniquely defined by the interface deformation; however, the structural solver is unaware of the fluid's incompressibility constraint, leaving the coupling procedure bound to fail [5, 6].

### 3.3. Update of Coupling Data

One countermeasure against the added-mass instability is to modify the coupling data in an update step before passing it on to the other solver. Typically, it is applied to the interface deformation. For that, the assignment  $\mathbf{d}^{k+1} = \tilde{\mathbf{d}}^k$  in step 4 of the Dirichlet-Neumann scheme is replaced by some update step  $\mathbf{d}^{k+1} = \mathcal{U}(\tilde{\mathbf{d}}^k)$ . But as the concept is applicable to other interface data too, it will be introduced for some generic interface field  $\tilde{\mathbf{x}}^k \in \mathbb{R}^m$  computed in iteration  $k$ , that is updated to the next iteration's input by  $\mathbf{x}^{k+1} = \mathcal{U}(\tilde{\mathbf{x}}^k)$ . The associated fixed-point residual  $\mathbf{R}^k = \tilde{\mathbf{x}}^k - \mathbf{x}^k$  quantifies the change of  $\mathbf{x}$  within coupling iteration  $k$ .

The simplest update is a *relaxation* of the coupling data,

$$\mathbf{x}^{k+1} = \mathcal{U}_{\text{Relax}}(\tilde{\mathbf{x}}^k) = \omega \tilde{\mathbf{x}}^k + (1 - \omega) \mathbf{x}^k, \quad (7)$$

where a relaxation factor  $0 < \omega \leq 1$  is required to increase stability ("under-relaxation"). Unfortunately, a fixed  $\omega$  often has to be chosen very small to ensure stability for all time steps, bringing along a drastic decrease in efficiency. Therefore, *Aitken's dynamic relaxation* [41, 43] adapts the relaxation factor in every coupling iteration by

$$\omega_k = -\omega_{k-1} \frac{(\mathbf{R}^{k-1})^T (\mathbf{R}^k - \mathbf{R}^{k-1})}{\|\mathbf{R}^k - \mathbf{R}^{k-1}\|_2^2} \quad (8)$$

before the update step (7). Despite its simplicity, Aitken's relaxation often significantly speeds up convergence. It can be interpreted as a simplified version of *interface quasi-Newton (IQN)* methods.

<sup>2</sup>The distinction between the output  $\tilde{\mathbf{d}}^k$  of the structural solver and the deformation field  $\mathbf{d}^{k+1}$  used as boundary condition in the flow problem is a preparation for the update step introduced in Section 3.3.

### 3.4. Interface Quasi-Newton Methods

Identifying the converged time step solution as a root of the fixed-point residual  $\mathbf{R}$ , convergence could be accelerated by using Newton's method as an update step, i.e.,

$$\mathbf{x}^{k+1} = \mathcal{U}_{\text{Newton}}(\tilde{\mathbf{x}}^k) = \tilde{\mathbf{x}}^k - \mathbf{J}_R^{-1}(\tilde{\mathbf{x}}^k) \mathbf{R}^k. \quad (9)$$

As the inverse Jacobian  $\mathbf{J}_R^{-1} := (d\mathbf{R}/d\tilde{\mathbf{x}})^{-1}$  is typically not accessible due to the required derivatives of the two solvers, interface quasi-Newton methods instead rely on an approximation  $\widehat{\mathbf{J}}_{-1} \approx \mathbf{J}_R^{-1} \in \mathbb{R}^{m \times m}$ .

It is based on multi-dimensional finite differences, forming the required data pairs  $(\Delta\tilde{\mathbf{x}}, \Delta\mathbf{R})$  from the intermediate fields  $\tilde{\mathbf{x}}^i$  and  $\mathbf{R}^i$  of the  $k$  coupling iterations already performed for the current time step. They are stored in the matrices  $\mathbf{V}_k \in \mathbb{R}^{m \times k}$  and  $\mathbf{W}_k \in \mathbb{R}^{m \times k}$  [12, 15]:

$$\mathbf{V}_k = [\Delta\mathbf{R}_{k-1}^k, \Delta\mathbf{R}_{k-2}^{k-1}, \dots, \Delta\mathbf{R}_0^1] \quad \text{with } \Delta\mathbf{R}_i^j = \mathbf{R}^j - \mathbf{R}^i, \quad (10a)$$

$$\mathbf{W}_k = [\Delta\tilde{\mathbf{x}}_{k-1}^k, \Delta\tilde{\mathbf{x}}_{k-2}^{k-1}, \dots, \Delta\tilde{\mathbf{x}}_0^1] \quad \text{with } \Delta\tilde{\mathbf{x}}_i^j = \tilde{\mathbf{x}}^j - \tilde{\mathbf{x}}^i. \quad (10b)$$

The collected data poses the constrained optimization problem

$$\min \|\widehat{\mathbf{J}}_{-1}\|_F \quad \text{subject to} \quad \widehat{\mathbf{J}}_{-1} \mathbf{V}_k = \mathbf{W}_k. \quad (11)$$

While the linear system alone would be underdetermined ( $m >> k$ ), the Frobenius norm minimization provides the unique solution  $\widehat{\mathbf{J}}_{-1} = \mathbf{W}_k (\mathbf{V}_k^T \mathbf{V}_k)^{-1} \mathbf{V}_k^T$ , that is inserted into Equation (9) to obtain the quasi-Newton update step

$$\mathbf{x}^{k+1} = \mathcal{U}_{\text{IQN}}(\tilde{\mathbf{x}}^k) = \tilde{\mathbf{x}}^k + \widehat{\mathbf{J}}_{-1}(-\mathbf{R}^k) = \tilde{\mathbf{x}}^k + \mathbf{W}_k \underbrace{(\mathbf{V}_k^T \mathbf{V}_k)^{-1} \mathbf{V}_k^T}_{:=\alpha^k} (-\mathbf{R}^k) = \tilde{\mathbf{x}}^k + \mathbf{W}_k \alpha^k. \quad (12)$$

Since we do not need the Jacobian explicitly, this update is evaluated by solving the least-squares problem

$$\min_{\alpha^k \in \mathbb{R}^k} \|\mathbf{V}_k \alpha^k + \mathbf{R}^k\|_2 \quad (13)$$

for the vector  $\alpha^k \in \mathbb{R}^k$ , e.g., using a QR decomposition via Householder reflections. In the first coupling iteration, when no data pairs are available yet, a relaxation step is used.

The technique outlined so far is the interface quasi-Newton *inverse least-squares (ILS)* method [12]. While its basic form only considers data collected during the current time step, the effectiveness of IQN methods is significantly improved by using data from past time steps too. A straightforward option is to explicitly include the data pairs of the  $q$  most recent time steps in  $\mathbf{V}_k$  and  $\mathbf{W}_k$ . But although proper filtering techniques can alleviate the issue, good choices of the parameter  $q$  are problem-dependent due to numerical challenges like bad conditioning, rank-deficiencies, and contradicting information [14].

As an alternative, multi-vector quasi-Newton methods reuse past data in an implicit manner [8, 15]: Formulating the new inverse Jacobian  ${}^{n+1}\widehat{\mathbf{J}}_{-1}$  as an update from that of the previous time step  ${}^n\widehat{\mathbf{J}}_{-1}$ , the Jacobian in the Frobenius norm minimization of Equation (11) is replaced by the increment:  $\min \|{}^{n+1}\widehat{\mathbf{J}}_{-1} - {}^n\widehat{\mathbf{J}}_{-1}\|_F$ . This results in the multi-vector approximation  ${}^{n+1}\widehat{\mathbf{J}}_{-1} = {}^n\widehat{\mathbf{J}}_{-1} + (\mathbf{W}_k - {}^n\widehat{\mathbf{J}}_{-1} \mathbf{V}_k) (\mathbf{V}_k^T \mathbf{V}_k)^{-1} \mathbf{V}_k^T$  and the update step

$$\mathbf{x}^{k+1} = \mathcal{U}_{\text{IQN}}(\tilde{\mathbf{x}}^k) = \tilde{\mathbf{x}}^k - {}^n\widehat{\mathbf{J}}_{-1} \mathbf{R}^k + (\mathbf{W}_k - {}^n\widehat{\mathbf{J}}_{-1} \mathbf{V}_k) \underbrace{(\mathbf{V}_k^T \mathbf{V}_k)^{-1} \mathbf{V}_k^T}_{\alpha^k} (-\mathbf{R}^k) = \tilde{\mathbf{x}}^k - {}^n\widehat{\mathbf{J}}_{-1} \mathbf{R}^k + (\mathbf{W}_k - {}^n\widehat{\mathbf{J}}_{-1} \mathbf{V}_k) \alpha^k. \quad (14)$$

Solving the same least squares problem as in Equation (13) for  $\alpha^k$ , the *implicit multi-vector least squares (IMVLS)* variant allows to evaluate this expression without any explicit Jacobian representation [16].

Aside from the references already given, the works by Lindner et al. [9] or Delaissé et al. [44] are recommended for an overview of different IQN methods.

### 3.5. Robin-Neumann Scheme

Despite the popularity of the Dirichlet-Neumann scheme, using the dynamic coupling condition to pass data from the fluid to the structure and the kinematic one for the way back is not without alternatives. As the Dirichlet condition of the flow problem is critical for both added-mass instability and the incompressibility dilemma, the *Robin-Neumann (RN)* scheme replaces it by a Robin condition that forms a linear combination of kinematic and dynamic continuity. Inserting the structure's velocity  $\mathbf{u}_s = \partial \mathbf{d}_s / \partial t$  and interface tractions  $\mathbf{T}_s \mathbf{n}_s$  on  $\Gamma_t^{fs}$ , Equation (2c) can be rearranged to

$$\mathbf{T}_f \mathbf{n}_f = \mathbf{T}_s \mathbf{n}_s + \alpha^{RN} \left( \frac{\partial \mathbf{d}_s}{\partial t} - \mathbf{u}_f \right) \quad \text{on } \Gamma_t^{fs} \quad \forall t \geq 0, \quad (15)$$

where the scalar parameter  $\alpha^{RN} > 0$  controls the weighting of the two contributions. In the limits, this condition reduces to a Neumann expression for  $\alpha^{RN} = 0$  and to a (weakly-imposed) Dirichlet condition for  $\alpha^{RN} \rightarrow \infty$ .

Typically, the tractions  $\mathbf{T}_s \mathbf{n}_s$  originate from the structural solution. But as their computation often requires reconstruction techniques or might even be impossible for a black box solver, we propose a different strategy: Due to the very nature of the structural problem as a dynamic balance of stresses, the structure's Cauchy tractions at the interface are already known before even calling the solver: They will balance the external loads, i.e., the fluid tractions passed to the structure<sup>3</sup>. Consequently, instead of explicitly computing any structural stress, these fluid tractions can directly be fed back into the Robin condition of the next iteration. The resulting coupling strategy is illustrated in Figure 2.

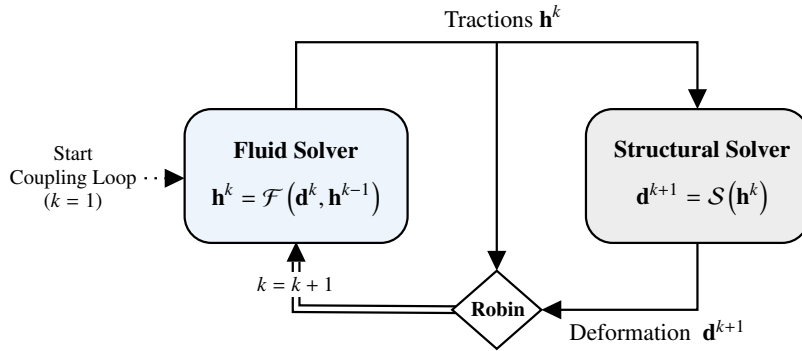


Figure 2: Robin-Neumann scheme with a direct feedback of fluid tractions into the Robin condition.

In coupling iteration  $k$ , the Robin condition then reads

$$\mathbf{T}_f \mathbf{n}_f = \mathbf{h}^{k-1} + \alpha^{RN} \left( \frac{\partial \mathbf{d}^k}{\partial t} - \mathbf{u}_f \right) \quad \text{on } \Gamma_t^{fs} \quad \forall t \geq 0. \quad (16)$$

The Robin-Neumann scheme not only reduces the added-mass instability, but also resolves the incompressibility dilemma. The key lies in weakening the Dirichlet condition of the flow problem, in principle allowing for a violation of kinematic continuity, but penalizing it with the factor  $\alpha^{RN}$ . Accordingly, the velocity difference of fluid and structure tends to zero as the coupling converges. To picture this, imagine the FSI interface is still moved with the structural deformation, but is no longer completely impermeable. Instead, an artificial flux through the boundary is permitted, so that the flow field always satisfies the incompressibility constraint. This way, fully-enclosed fluid problems are unproblematic, since numerically, they are no longer of pure-Dirichlet type. Concerning the added-mass effect, the artificial permeability caps the direct link between overestimated deformations and excessive inertia terms, as the flow no longer “blindly” follows the interface; this lowers the risk of a reciprocal amplification and increases stability.

Unfortunately, these strengths are put into perspective by the main drawback of the Robin-Neumann scheme, i.e., its dependence on the Robin parameter. While decreasing  $\alpha^{RN}$  stabilizes the coupling by weighting the Neumann contribution, it slows down convergence and reduces the solution quality. For growing values of  $\alpha^{RN}$ , in contrast, the

<sup>3</sup>Technically, this equality only holds if the structural subproblem has fully converged. For other cases, it is still a very good approximation.

accentuated Dirichlet part magnifies the added-mass instability. Moreover, it gradually reintroduces the incompressibility dilemma for fully-enclosed problems by a stricter penalization of deviations from kinematic continuity.

Good choices of  $\alpha^{RN}$  balance out these two opposing trends, but are very difficult to determine a priori. Various highly recommendable works study the effect of the Robin parameter in detail, like Badia et al. [19], Gerardo-Giorda et al. [21], Cao et al. [22, 23], or Gigante and Vergara [24]. Analyzing simplified FSI problems, for example potential or inviscid flows interacting with linear beam or membrane models, they derive suggestions for choosing  $\alpha^{RN}$ , including both constant values and spatially varying expressions [23]. Despite their undisputed importance, these formulations depend on a broad set of parameters, such as material properties, geometry, and time step size. Beyond that, they typically have a limited applicability to more general problems, so that choosing the best Robin parameter is still an ongoing research topic.

However, as the numerical results in Section 5 will demonstrate, the quasi-Newton acceleration proposed in this work substantially reduces the impact of the Robin parameter, and with it the urgency of finding a good choice.

*Remark 1:* Although referring to tractions so far, passing stress tensors or forces from fluid to structure works analogously. In our finite-element framework, we transfer consistent nodal forces, which are computed from integrating the tractions over the FSI interface [40]. The same force term can be identified in the finite-element boundary integral of the Robin condition, reading (with the test functions  $\mathbf{w}_f$ )

$$\int_{\Gamma_t^{fs}} \mathbf{w}_f \mathbf{T}_f \mathbf{n}_f d\Gamma = \underbrace{\int_{\Gamma_t^{fs}} \mathbf{w}_f \mathbf{h}^{k-1} d\Gamma}_{\mathbf{F}^{k-1}} + \int_{\Gamma_t^{fs}} \mathbf{w}_f \alpha^{RN} \left( \frac{\partial \mathbf{d}^k}{\partial t} - \mathbf{u}_f \right) d\Gamma = \mathbf{F}^{k-1} + \int_{\Gamma_t^{fs}} \mathbf{w}_f \alpha^{RN} \left( \frac{\partial \mathbf{d}^k}{\partial t} - \mathbf{u}_f \right) d\Gamma, \quad (17)$$

so that the direct feedback of fluid loads is applicable to the nodal forces  $\mathbf{F}^k$ , too.

#### 4. Robin-Neumann Quasi-Newton (RN-QN) Scheme

Despite being inherently different concepts, both the Robin-Neumann scheme and interface quasi-Newton methods can improve the coupling's stability and efficiency. The main motivation of this work is to combine the two approaches and benefit from their respective strengths. We therefore propose the following *Robin-Neumann quasi-Newton (RN-QN)* scheme illustrated in Figure 3:

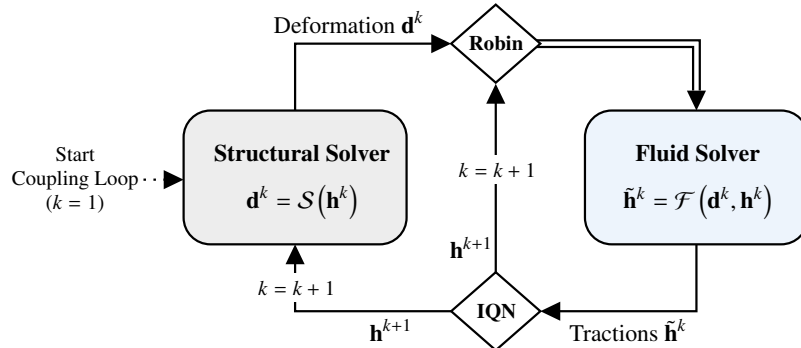


Figure 3: Sketch of the proposed RN-QN scheme which combines the Robin-Neumann approach with an interface quasi-Newton acceleration. Key features are the quasi-Newton update of the fluid loads and their direct feedback into the fluid's Robin condition.

Essentially, the Robin-Neumann scheme as presented in Section 3.5 is extended by an IQN method. Updating the interface deformation, however, would conflict with feeding back the fluid tractions, as the Dirichlet and Neumann contributions of the Robin condition would be inconsistent. Therefore, the quasi-Newton step modifies the fluid loads instead. The resulting updated tractions  $\mathbf{h}^{k+1} = \mathcal{U}_{IQN}(\tilde{\mathbf{h}}^k)$  enter both the structural solver and the fluid's Robin boundary condition in the next iteration. Lastly, the order of the two solver calls has been switched, as the collection of input-output data slightly profits from performing the quasi-Newton update in the end of a coupling iteration.

The new procedure is outlined in Algorithm 1: Coupling iteration  $k$  starts with the structural solver computing the deformation  $\mathbf{d}^k = \mathcal{S}(\mathbf{h}^k)$ , which is combined with the tractions  $\mathbf{h}^k$  to form a Robin condition. With that, the flow solver determines new tractions  $\tilde{\mathbf{h}}^k = \mathcal{F}(\mathbf{d}^k, \mathbf{h}^k)$ . After the quasi-Newton step  $\mathbf{h}^{k+1} = \mathcal{U}_{IQN}(\tilde{\mathbf{h}}^k)$ , the updated tractions  $\mathbf{h}^{k+1}$  are passed back to the structure and stored for the next iteration's Robin term.

---

**Coupling loop:** **for**  $k = 1, \dots$  *until convergence* **do**

Call structural solver:

$$\mathbf{d}^k = \mathcal{S}(\mathbf{h}^k)$$

Pass deformation unaltered:

$$\mathbf{d}^k$$

Form Robin condition:

$$\mathbf{T}_f \mathbf{n}_f = \mathbf{h}^k + \alpha^{RN} \left( \frac{\partial \mathbf{d}^k}{\partial t} - \mathbf{u}_f \right)$$

Call fluid solver:

$$\tilde{\mathbf{h}}^k = \mathcal{F}(\mathbf{d}^k, \mathbf{h}^k)$$

IQN update of fluid loads:

$$\mathbf{h}^{k+1} = \mathcal{U}_{IQN}(\tilde{\mathbf{h}}^k)$$

Pass loads to structure and store for Robin condition:

$$\mathbf{h}^{k+1}$$

**end**

Set initial tractions of next time step:  $\mathbf{h}^1 = \mathbf{h}^{k+1}$

---

Algorithm 1: Pseudo-code of the new RN-QN scheme. The outlined procedure is repeated for every time step.

*Remark 2:* Depending on which data field is sent, the quasi-Newton step can equivalently be performed on tractions, stress tensors, or forces. Note, however, that updating stress tensors might affect the conditioning of the least-squares problem negatively due to the typically very different scales of shear stresses and pressure. For the numerical examples in Section 5, the consistent nodal forces (see Remark 1) are fed into the IQN method.

*Remark 3:* The idea to switch the order of solver calls and apply the quasi-Newton step to the fluid loads rather than the interface deformation, as done for the RN-QN scheme, is just as well applicable to the Dirichlet-Neumann approach. The performance analysis of different coupling schemes in Section 5 will therefore include this variant, labeling it  $DN\text{-}IQN_f$ , as opposed to  $DN\text{-}IQN_s$  for the classical update of deformations.

## 5. Numerical Examples

This section investigates the performance of the new quasi-Newton-accelerated Robin-Neumann scheme in two steps: First, its superiority over the plain Robin-Neumann scheme is shown for two enclosed-fluid problems, for which the Dirichlet-Neumann scheme is not applicable. Afterwards, the RN-QN scheme is compared to the Dirichlet-Neumann scheme with IQN update for an open fluid configuration.

*Remark 4:* The computational cost per coupling iteration is virtually the same for all partitioned schemes discussed in this work, i.e., Dirichlet-Neumann and Robin-Neumann variants with or without quasi-Newton update. That is because the solver calls are expensive enough to render the differences negligible, which is in line with literature [15, 16]. Consequently, in the following a scheme's efficiency will be assessed by the coupling iterations required.

### 5.1. Inflating Balloon

The first test case considers the inflating 2D water balloon depicted in Figure 4: A flexible ring structure is filled with an incompressible fluid. Due to a time-dependent in-/outflow condition at the interior fluid boundary, the balloon will be in- and deflating [27, 39]. The parameters are listed in Table 1. Note in particular the high density ratio of  $\rho_f/\rho_s = 1.0$ , which hints at a pronounced added-mass instability.

Since the symmetric inflow condition is known, the balloon volume, and hence the radius, can be computed analytically. Taking into account the geometrical error introduced by approximating the circular FSI interface with  $n$  linear segments, the analytical radius is:

$$R_{\text{Polygon}}(t) = \sqrt{R_0^2 + \frac{2\pi r}{\frac{n}{2} \sin \frac{2\pi}{n}} \int_0^t U_{in}(\bar{t}) d\bar{t}}. \quad (18)$$

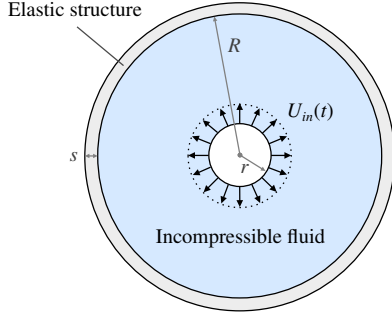


Figure 4: Sketch of the inflating balloon case.

Parameter	Variable	Magnitude	Dimension
Inner radius	$r$	0.05	[L]
Initial outer radius	$R_0$	0.28	[L]
Fluid density	$\rho_f$	1000.0	[M L <sup>-3</sup> ]
Dynamic fluid viscosity	$\mu_f$	1.0	[M L <sup>-1</sup> T <sup>-1</sup> ]
Normal inflow velocity	$U_{in}(t)$	$10 \sin(\pi t)$	[M L <sup>-1</sup> ]
Structural density	$\rho_s$	1000.0	[M L <sup>-3</sup> ]
Young's modulus	$E_s$	$1.4 \cdot 10^6$	[M L <sup>-1</sup> T <sup>-1</sup> ]
Poisson ratio	$\nu_s$	0.3	-
Wall thickness	$s$	0.02	[L]

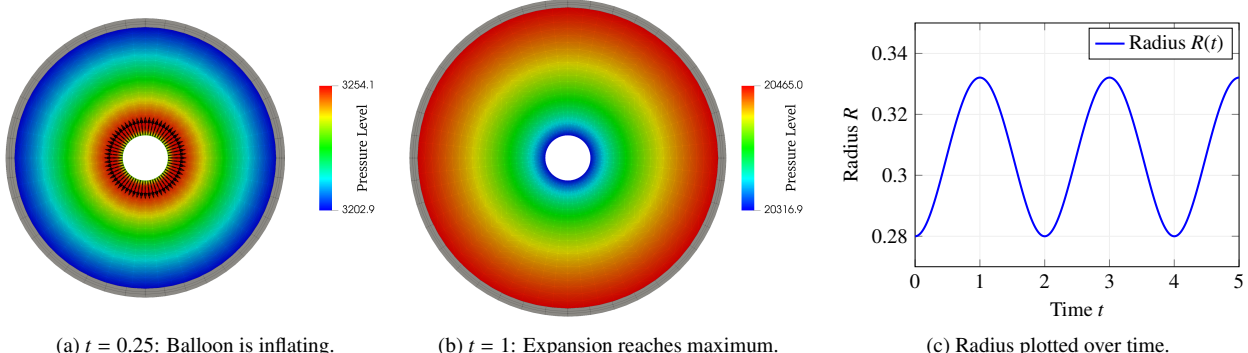
Table 1: Parameters of the inflating balloon test case.

In this case, the interface is discretized by  $n = 60$  edges of the fluid mesh, which in total consists of 2400 triangular finite elements with 1260 nodes. The elastic structure is meshed by  $40 \times 3 = 120$  nonlinear quadrilateral isogeometric elements, that are defined on a second-degree NURBS with 225 control points. The simulated time span of  $t_{end} = 5.0$  is divided into  $n_{ts} = 500$  steps of size  $\Delta t = 0.01$ .

As discussed in Section 3.1, the convergence criterion takes both the coupling loop and the Newton steps of the subproblems into account. The bounds for this test case are  $\varepsilon_{Coupling} = 10^{-6}$  and  $\varepsilon_{Problem} = 10^{-10}$  for both problems.

### 5.1.1. Results

Due to the inflow over the boundary and the incompressibility constraint, the fluid domain is expanding, causing a widening of the elastic structure. As soon as the boundary flux is switching to an outflow condition, the system starts shrinking again. Figure 5 visualizes this in- and deflation by two snapshots and a plot of the balloon radius over time.



(a)  $t = 0.25$ : Balloon is inflating. (b)  $t = 1$ : Expansion reaches maximum. (c) Radius plotted over time.

Figure 5: Illustration of the balloon's in- and deflation three snapshots.

The focus of this work, however, is less on the simulation results themselves than on the performance of different FSI coupling strategies. Due to the pure-Dirichlet character of the fluid problem, the Dirichlet-Neumann scheme is not applicable to this test case. Instead, Table 2 compares multiple variants of the Robin-Neumann scheme: With or without quasi-Newton acceleration and for various choices of the parameter  $\alpha^{RN}$ . For the RN-QN method, three different update techniques are listed: (1) The IQN-IMVLS method with an implicit reutilization of past data, (2) the IQN-ILS approach without any past data, and (3) Aitken's dynamic relaxation. Aside from the average number of coupling iterations required per time step, the violation of the kinematic constraint is compared. It is quantified via the relative artificial flux through the FSI interface in the simulated time span  $[0, t_{end}]$ , i.e.,

$$\varepsilon_{rel} = \int_0^{t_{end}} \frac{|\dot{V}^{fs}(t)|}{V(t)} dt \quad \text{with } \dot{V}^{fs}(t) = \int_{\Gamma_t^{fs}} \left| \left( \frac{\partial \mathbf{d}_s}{\partial t} - \mathbf{u}_f \right) \cdot \mathbf{n} \right| d\Gamma \quad \text{and } V(t) = V_0 + \int_0^t \sum \dot{V}(\bar{t}) d\bar{t}. \quad (19)$$

This measure is chosen rather than the averaged relative deviation from the analytical radius, as the latter is dominated by the simulation's temporal discretization error and therefore virtually the same for all runs (about  $8.6 \cdot 10^{-5}$ ).

Coupling scheme	Coupling iterations per time step							
	Relative artificial flux							
	$\alpha^{RN} =$	$10^3$	$10^4$	$5 \cdot 10^4$	$10^5$	$5 \cdot 10^5$	$10^6$	$10^7$
<b>Robin-Neumann</b>	<b>350.77</b>	<b>43.29</b>	<b>8.98</b>	—	—	—	—	—
	1.07E-3	1.40E-4	2.98E-5	—	—	—	—	—
<b>RN-QN (IMVLS)</b>	<b>6.22</b>	<b>5.25</b>	<b>5.16</b>	<b>5.12</b>	<b>5.10</b>	<b>5.13</b>	<b>5.54</b>	—
	1.06E-3	1.43E-4	2.98E-5	1.50E-5	3.00E-6	1.50E-6	1.50E-7	—
<b>RN-QN (ILS, <math>q = 0</math>)</b>	<b>18.85</b>	<b>8.21</b>	<b>6.28</b>	<b>6.22</b>	<b>6.04</b>	<b>7.25</b>	<b>11.50</b>	—
	1.06E-3	1.43E-4	2.98E-5	1.50E-5	3.00E-6	1.50E-6	1.50E-7	—
<b>RN-QN (Aitken)</b>	<b>41.6</b>	<b>10.34</b>	<b>6.91</b>	<b>7.82</b>	<b>9.10</b>	<b>10.87</b>	<b>15.38</b>	—
	1.03E-3	1.43E-4	2.98E-5	1.50E-5	3.02E-6	1.50E-6	1.49E-7	—

Table 2: Comparison of the plain Robin-Neumann and the new RN-QN scheme for the inflating balloon test case. For RN-QN, the employed update scheme is indicated in brackets. The **bold numbers** indicate the average number of coupling iterations required per time step, the gray values refer to the relative artificial flux  $\varepsilon_{rel}$  as defined in Equation (19). Missing values indicate that a converged solution could not be obtained.

The first row shows both the main strength and the biggest shortcoming of the Robin-Neumann scheme: Although it is in principle capable of yielding efficient and accurate results, its performance massively depends on the choice of the Robin parameter. Away from some acceptable range, small values lead to an impractically slow convergence; picking  $\alpha^{RN}$  bigger than some critical bound, on the other hand, causes the coupling iteration to diverge altogether.

In contrast, the results of the new Robin-Neumann scheme with quasi-Newton acceleration show only a small dependency on  $\alpha^{RN}$ . In fact, a very wide parameter range yields a similar convergence rate that even outperforms the plain Robin-Neumann scheme with an optimal parameter. Consequently, the further  $\alpha^{RN}$  moves away from the optimum, the more substantial the relative speed-up of the new RN-QN coupling scheme gets.

Aside from performance, Table 2 also indicates how increasing the Robin parameter improves the solution quality, i.e., the conformity with kinematic continuity. As expected for a penalty-enforced constraint, the magnitude of the remaining artificial flux is solely determined by the choice of  $\alpha^{RN}$  and unaffected by the quasi-Newton update.

Comparing the update techniques employed within the RN-QN approach, it should be noted: (1) The convergence rate clearly benefits from reusing past time step data in the quasi-Newton update, e.g., via the IQN-IMVLS method. (2) Despite being less effective than a quasi-Newton technique, Aitken's relaxation is still an easily implemented option to start with in case no IQN framework is available yet.

All in all, this test case clearly indicates that the new RN-QN scheme is preferable to the standard Robin-Neumann coupling, as it strongly speeds up convergence and substantially reduces the dependency on the Robin parameter  $\alpha^{RN}$ .

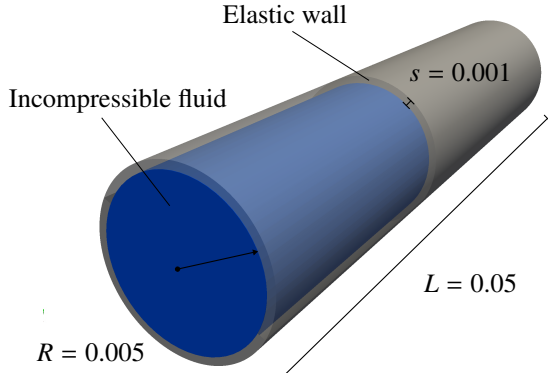
## 5.2. Elastic Tube

The next test case considers the cylindrical pipe filled with an incompressible fluid depicted in Figure 6a. Due to a short excitation in the beginning, a deformation wave will propagate through the elastic channel wall. Note that unlike in similar cases from literature [7, 9], this excitation is not introduced via a pressure boundary condition. Instead, a high inflow velocity is prescribed for a short time at one end of the pipe. This modification allows to switch between two scenarios simply by changing the boundary condition at the opposite end of the pipe: It will either (1) be closed to form a pure-Dirichlet problem or (2) allow for free outflow via a natural Neumann condition.

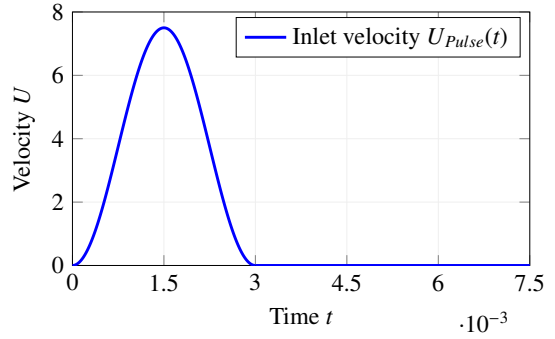
The tube has the inner radius  $R = 0.005$ , wall thickness  $s = 0.001$ , and length  $L = 0.05$ . The fluid density is  $\rho_f = 1000.0$  and its dynamic viscosity  $\mu_f = 0.003$ . The elastic wall is characterized by the density  $\rho_s = 1000.0$ , Young's modulus  $E_s = 3.0 \cdot 10^5$ , and a Poisson ratio of  $\nu_s = 0.3$ , so that the density ratio is again  $\rho_f/\rho_s = 1.0$ .

At the channel inlet, a parabolic inflow velocity profile with a time-dependent magnitude is prescribed as

$$U_{in}(r, t) = \frac{(R - r)(R + r)}{R^2} U_{pulse}(t) \quad \text{with} \quad U_{pulse}(t) \begin{cases} 3.75 \left(1 - \cos\left(\frac{2\pi}{0.003}t\right)\right) & \text{if } t \leq 0.003, \\ 0 & \text{if } t > 0.003, \end{cases} \quad (20)$$



(a) Sketch of the elastic tube test case.



(b) Inlet velocity  $U_{\text{Pulse}}$  plotted over time.

Figure 6: Elastic tube test case

where  $r$  is the radial coordinate direction. As the plot of  $U_{\text{pulse}}(t)$  in Figure 6b visualizes, the inflow velocity is ramped up and down over a short period of time.

On account of its symmetry in circumferential direction, the simulation is run on a  $90^\circ$  section of the cylindrical domain only. The fluid mesh consists of 14 326 linear Lagrangian tetrahedral elements with 3380 nodes and is refined close to the walls and the inlet. The elastic channel wall is clamped at both ends and discretized by  $6 \times 30 = 180$  nonlinear isogeometric Reissner-Mindlin shell elements [45] on a degree-2 NURBS surface with 256 control points.

The simulation is run for 300 time steps of size  $\Delta t = 2.5 \cdot 10^{-5}$ . The convergence bounds are again  $\varepsilon_{\text{Coupling}} = 10^{-6}$  and  $\varepsilon_{\text{Problem}} = 10^{-10}$ .

### 5.2.1. Results

The elastic tube case is studied for two separate versions, that differ in the boundary conditions: (1) In the first configuration, the end of the pipe is closed by a rigid wall, i.e., a fluid velocity of zero is prescribed. Consequently, it again poses a fully-enclosed problem the Dirichlet-Neumann scheme cannot handle. (2) The second case uses a free outflow condition at the pipe's end. The results of both variants are illustrated in Figure 7 by three snapshots. As expected, the increasing inflow velocity causes a widening of the tube close to the inlet. When the velocity is reduced again, this deformation starts to propagate like a wave through the elastic structure. Qualitatively, a difference between the two configurations can mainly be observed towards the end of the simulation, when the deformation pulse reaches the opposite end of the tube.

In the following, focus is again put on comparing the performance of different coupling schemes for both setups.

#### Closed End

Looking at the results of various Robin-Neumann variants for the closed configuration in Table 3, similar conclusions as for the previous test case can be drawn: Again, the potential of the standard Robin-Neumann scheme is strongly compromised by its distinct sensitivity to the parameter  $\alpha^{RN}$ . This very sensitivity is substantially reduced by the RN-QN scheme, as it widely extends the parameter range that leads to fast convergence. Accordingly, the efficiency gains are more significant for non-optimal values of  $\alpha^{RN}$ , but the new RN-QN scheme outperforms the plain Robin-Neumann approach for all choices. It is worth noting that these major improvements come without any significant drawbacks. Similar to the balloon test case, the accuracy of all Robin-Neumann variants is decreasing for lower values of  $\alpha^{RN}$ , independently from the quasi-Newton update. However, the artificial flux is rather small for all simulations.

Again, an IQN method taking into account past time step data, like the IMVLS approach, is the most effective choice. Nevertheless, again two alternatives are listed since their results point out the effects of poor choices for  $\alpha^{RN}$ : (1) If the parameter is too small, convergence is slowed down by putting unnecessary weight on the Neumann term of the Robin condition. Without past time step data, the quasi-Newton update struggles to a similar extent as Aitken's relaxation to accelerate the coupling. (2) Choosing  $\alpha^{RN}$  too high, on the other hand, increases the added-mass instability, for which in general quasi-Newton methods are known to perform better than Aitken's relaxation [16].

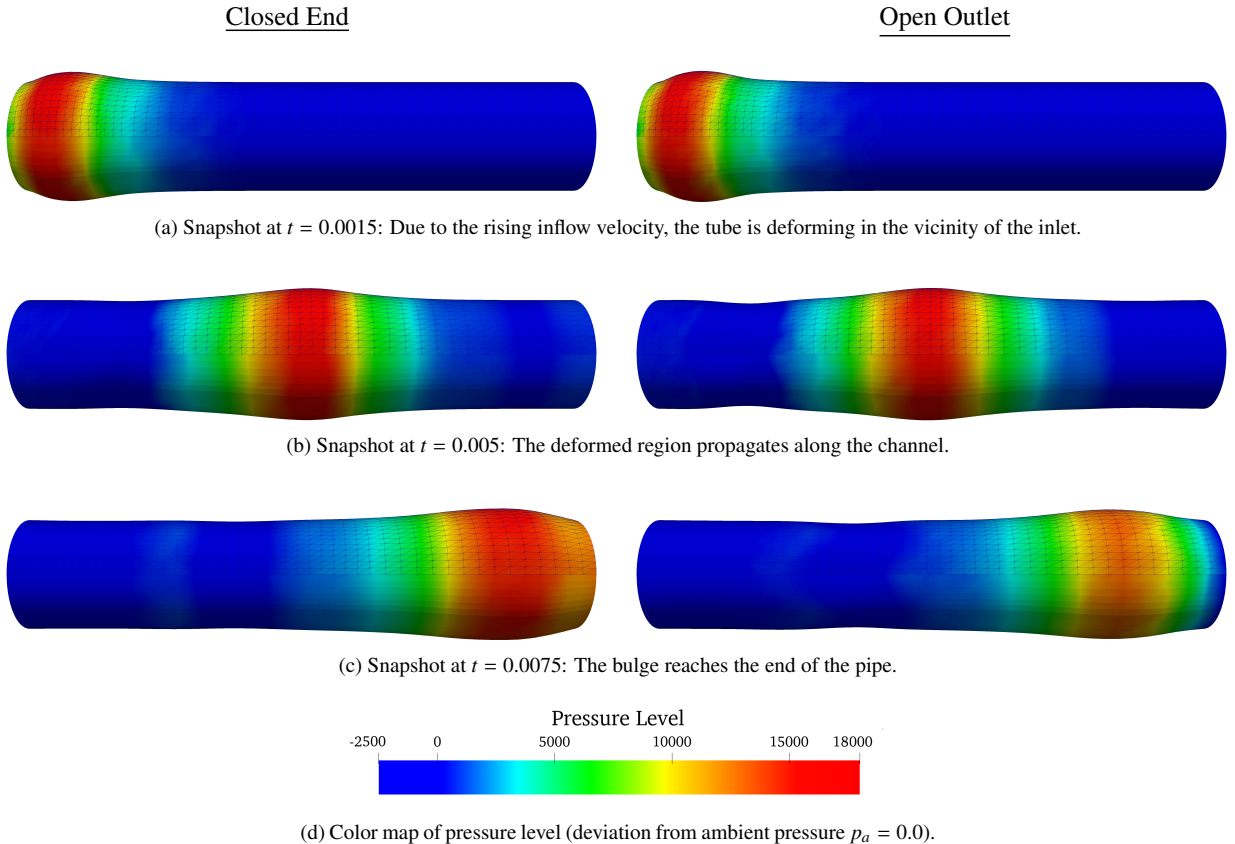


Figure 7: Illustration of the deformation wave running through the tube for both test case versions. While the upper part of the pipe is the actual fluid mesh, the lower half follows from symmetry and is only shown for a better visualization. Coloring is based on the fluid's pressure field.

Independent from the specific update technique, the Robin parameter shows an upper bound beyond which no stable results are obtained due to the incompressibility dilemma, as discussed in the next section.

In summary, the closed tube test case reinforces the key take-away of Section 5.1, that is the superiority of the RN-QN scheme over the Robin-Neumann approach without update step.

Coupling scheme	Coupling iterations per time step								
	Relative artificial flux								
$\alpha^{RN} =$	$10^3$	$10^4$	$5 \cdot 10^4$	$10^5$	$5 \cdot 10^5$	$10^6$	$10^7$	$10^8$	$10^9$
<b>Robin-Neumann</b>	<b>428.81</b>	<b>61.27</b>	<b>13.27</b>	<b>8.46</b>	—	—	—	—	—
	4.83E-3	8.84E-4	2.23E-4	1.19E-4	—	—	—	—	—
<b>RN-QN (IMVLS)</b>	<b>9.85</b>	<b>6.99</b>	<b>5.27</b>	<b>4.83</b>	<b>6.63</b>	<b>7.07</b>	<b>8.46</b>	<b>13.47</b>	—
	4.80E-3	8.67E-4	2.18E-4	1.16E-4	2.51E-5	1.27E-5	1.29E-6	1.29E-7	—
<b>RN-QN (ILS, <math>q = 0</math>)</b>	<b>48.68</b>	<b>17.80</b>	<b>8.73</b>	<b>7.28</b>	<b>14.05</b>	<b>14.81</b>	<b>16.58</b>	<b>18.28</b>	—
	4.87E-3	8.67E-4	2.18E-4	1.16E-4	2.51E-5	1.27E-5	1.29E-6	1.29E-7	—
<b>RN-QN (Aitken)</b>	<b>57.34</b>	<b>21.09</b>	<b>10.90</b>	<b>8.59</b>	<b>18.94</b>	<b>24.29</b>	<b>61.79</b>	<b>90.41</b>	—
	4.88E-3	8.85E-4	2.18E-4	1.16E-4	2.51E-5	1.27E-5	1.31E-6	1.30E-7	—

Table 3: Comparison of various Robin-Neumann schemes for the closed tube test case. Again **bold numbers** are the average coupling iterations per time step, while the gray values quantify accuracy via  $\varepsilon_{rel}$  as defined in Equation (19). Missing values indicate no stable results were found.

### Open Outlet

So far, this work compared the new RN-QN scheme to the pure Robin-Neumann coupling for two fully-enclosed cases. For general FSI problems without fully-enclosed fluids, however, the Dirichlet-Neumann scheme with interface quasi-Newton acceleration is the prevalent partitioned algorithm. Aside from multiple Robin-Neumann variants, the performance analysis in Table 4 of the tube with open outlet therefore also lists two Dirichlet-Neumann schemes with quasi-Newton update: As discussed in Remark 3, the update is applied to either the interface deformation, labeled as  $DN\text{-IQN}_s$ , or the fluid forces,  $DN\text{-IQN}_f$ .

Coupling scheme	Coupling iterations per time step									
	Relative artificial flux									
<b>DN-IQN<sub>s</sub> (IMVLS)</b>	<b>9.54</b> 4.27E-12									
<b>DN-IQN<sub>f</sub> (IMVLS)</b>	<b>8.43</b> 1.16E-19									
$\alpha^{RN} =$	10 <sup>3</sup>	10 <sup>4</sup>	5 · 10 <sup>4</sup>	10 <sup>5</sup>	5 · 10 <sup>5</sup>	10 <sup>6</sup>	10 <sup>7</sup>	10 <sup>10</sup>	10 <sup>18</sup>	
<b>Robin-Neumann</b>	<b>431.89</b> 5.03E-3	<b>62.27</b> 9.28E-4	<b>12.57</b> 2.39E-4	<b>8.33</b> 1.28E-4	—	—	—	—	—	
<b>RN-QN (IMVLS)</b>	<b>11.39</b> 5.00E-3	<b>6.91</b> 9.00E-4	<b>5.35</b> 2.31E-4	<b>4.82</b> 1.23E-4	<b>6.55</b> 2.67E-5	<b>7.10</b> 1.35E-5	<b>8.36</b> 1.37E-6	<b>9.68</b> 1.37E-8	<b>9.70</b> 1.30E-12	

Table 4: Performance comparison of different partitioned algorithms for the open tube test case, including both Robin-Neumann and Dirichlet-Neumann variants. (The coloring and formatting is equivalent to Table 2 and Table 3.)

First of all, looking only at the Robin-based approaches, the same advantages of the new RN-QN approach over the plain Robin-Neumann scheme as for the two previous test cases are observed. A major difference, however, is that in this test case the RN-QN coupling does not have any apparent upper bound for the Robin parameter. That is because as discussed in Section 3.5, increasing  $\alpha^{RN}$  brings the Robin-Neumann approach closer to the Dirichlet-Neumann scheme, entailing its two main shortcomings: Aside from the growing added-mass effect, which is kept under control by the quasi-Newton update, the increased penalization of violating kinematic continuity essentially reintroduces the incompressibility dilemma. As a consequence, the upper bound for the RN-QN scheme only exists in case of pure-Dirichlet problems, since they in general cannot satisfy both kinematic continuity and incompressibility at the same time. For other FSI problems, like the tube with open outlet, the incompressibility constraint will always be fulfilled, so that kinematic continuity can be enforced by a very high Robin parameter without loosing stability.

The two Dirichlet-Neumann variants both yield good performance. It is interesting to see that the  $DN\text{-IQN}_f$  algorithm converges slightly faster than the more traditional  $DN\text{-IQN}_s$  variant. An explanation could be that in this test case it is a better initial guess to start a new time step with the same loads acting on the structural body, rather than the fluid experiencing the same boundary velocity as in the previous time step.

Note that even for the Dirichlet-Neumann scheme the two solution fields will be consistent only up to a limited precision, due to its staggered nature: No matter when the iteration loop is left, one solution field was inevitably updated more recently than the other. For the  $DN\text{-IQN}_s$  variant, the structural solver is called last, resulting in the negligible, though nonzero artificial flux seen in Table 4. In contrast, the  $DN\text{-IQN}_f$  procedure exactly (within floating-point arithmetic) satisfies kinematic continuity, but has a marginal offset in the interface tractions. Analogously, the RN-QN scheme's velocity difference is originating only from the Robin condition, not the staggered iteration.

The main focus of this test case, however, is to compare the new RN-QN scheme to the quasi-Newton-accelerated Dirichlet-Neumann approach: It becomes apparent that for almost the complete parameter range covered in the study, the RN-QN coupling keeps up in terms of efficiency. For good choices of  $\alpha^{RN}$ , it actually converges significantly faster. Setting  $\alpha^{RN} = 10^5$  yields the biggest speed-up of roughly 50%. Despite the slight error in kinematic continuity inherent to Robin-Neumann variants, these results of the RN-QN method are remarkable, considering the widespread usage of the Dirichlet-Neumann coupling with quasi-Newton update in partitioned fluid-structure interaction.

## 6. Conclusion

This work presents a novel coupling strategy for partitioned fluid-structure interaction that merges the Robin-Neumann scheme with interface quasi-Newton methods. As confirmed by the numerical examples in Section 5, the *Robin-Neumann quasi-Newton (RN-QN)* scheme benefits from the individual strengths of both its ingredients: Being a Robin-Neumann approach, it can handle FSI simulations involving fully-enclosed incompressible fluids and is less prone to the added-mass effect. The main drawback of the Robin-Neumann concept, i.e., its distinct sensitivity to the Robin weighting parameter  $\alpha^{RN}$ , on the other hand, is mitigated by the integrated quasi-Newton update. It does not only accelerate the coupling's convergence substantially, but also widely extends the parameter range of  $\alpha^{RN}$  that produces stable results at all. Consequently, finding a good choice of the Robin parameter is far less critical.

Aside from that, the proposed direct feedback of fluid loads into the Robin condition renders any explicit computation of structural Cauchy stresses obsolete and hence strongly facilitates the usage of Robin-Neumann schemes, in particular for black box solvers.

The comparison of different coupling algorithms in Section 5 clearly shows the new RN-QN scheme is by all means preferable to the standard Robin-Neumann approach, without introducing any drawbacks of its own. Therefore, it is in particular beneficial for FSI simulations involving pure-Dirichlet fluid problems, since in that case none of the Dirichlet-Neumann-based schemes provides an alternative. Beyond that, the open tube test case allows to compare the new coupling algorithm to the predominant partitioned approach for fluid-structure interaction, i.e., the Dirichlet-Neumann scheme with an interface quasi-Newton update. In a remarkable manner, the RN-QN scheme not only keeps up for a very wide range of parameters, but for good choices of  $\alpha^{RN}$  even outperforms it significantly. These results demonstrate the potential of the new coupling to provide superior convergence speed.

In summary, the proposed *Robin-Neumann quasi-Newton (RN-QN)* scheme is a new efficient and stable partitioned algorithm for fluid-structure interaction, which in addition is capable of handling fully-enclosed incompressible fluids.

## Acknowledgement

The authors gratefully acknowledge the computing time granted by the JARA Vergabegremium and provided on the JARA Partition part of the supercomputer CLAIX at RWTH Aachen University. This work is funded by the Federal Ministry of Education and Research (BMBF) and the state of North Rhine-Westphalia as part of the NHR Program.

## References

- [1] P. Causin, J.-F. Gerbeau, F. Nobile, Added-mass effect in the design of partitioned algorithms for fluid–structure problems, *Computer Methods in Applied Mechanics and Engineering* 194 (42-44) (2005) 4506–4527. doi:10.1016/j.cma.2004.12.005.
- [2] C. Förster, Robust methods for fluid-structure interaction with stabilised finite elements, Ph.D. thesis, University of Stuttgart (2007). doi:10.18419/opus-270.
- [3] C. Förster, W. A. Wall, E. Ramm, Artificial added mass instabilities in sequential staggered coupling of nonlinear structures and incompressible viscous flows, *Computer Methods in Applied Mechanics and Engineering* 196 (7) (2007) 1278–1293. doi:10.1016/j.cma.2006.09.002.
- [4] E. H. van Brummelen, Added mass effects of compressible and incompressible flows in fluid-structure interaction, *Journal of Applied Mechanics* 76 (2) (2009) 021206. doi:10.1115/1.3059565.
- [5] U. Kättler, C. Förster, W. A. Wall, A solution for the incompressibility dilemma in partitioned fluid–structure interaction with pure Dirichlet fluid domains, *Computational Mechanics* 38 (4) (2006) 417–429. doi:10.1007/s00466-006-0066-5.
- [6] A. E. J. Bogaers, S. Kok, B. D. Reddy, T. Franz, Extending the robustness and efficiency of artificial compressibility for partitioned fluid–structure interactions, *Computer Methods in Applied Mechanics and Engineering* 283 (2015) 1278–1295. doi:10.1016/j.cma.2014.08.021.
- [7] J. Degroote, R. Haelterman, S. Annerel, P. Bruggeman, J. Vierendeels, Performance of partitioned procedures in fluid–structure interaction, *Computers & Structures* 88 (7-8) (2010) 446–457. doi:10.1016/j.compstruc.2009.12.006.
- [8] A. E. J. Bogaers, S. Kok, B. D. Reddy, T. Franz, Quasi-Newton methods for implicit black-box FSI coupling, *Computer Methods in Applied Mechanics and Engineering* 279 (2014) 113–132. doi:10.1016/j.cma.2014.06.033.
- [9] F. Lindner, M. Mehl, K. Scheufele, B. Uekermann, A comparison of various quasi-Newton schemes for partitioned fluid-structure interaction, in: *Coupled VI: Proceedings of the VI International Conference on Computational Methods for Coupled Problems in Science and Engineering*, CIMNE, 2015, pp. 477–488.
- [10] J.-F. Gerbeau, M. Vidrascu, A quasi-Newton algorithm based on a reduced model for fluid-structure interaction problems in blood flows, *ESAIM: Mathematical Modelling and Numerical Analysis* 37 (4) (2003) 631–647. doi:10.1051/m2an:2003049.

[11] E. H. van Brummelen, C. Michler, R. de Borst, Interface-GMRES (R) acceleration of subiteration for fluid-structure-interaction problems, Report Dacs-05-001 (2005).

[12] J. Degroote, K.-J. Bathe, J. Vierendeels, Performance of a new partitioned procedure versus a monolithic procedure in fluid–structure interaction, *Computers & Structures* 87 (11-12) (2009) 793–801. doi:10.1016/j.compstruc.2008.11.013.

[13] J. Degroote, J. Vierendeels, Multi-solver algorithms for the partitioned simulation of fluid–structure interaction, *Computer Methods in Applied Mechanics and Engineering* 200 (25-28) (2011) 2195–2210. doi:10.1016/j.cma.2011.03.015.

[14] R. Haelterman, A. E. J. Bogaers, K. Scheufele, B. Uekermann, M. Mehl, Improving the performance of the partitioned QN-ILS procedure for fluid–structure interaction problems: Filtering, *Computers & Structures* 171 (2016) 9–17. doi:10.1016/j.compstruc.2016.04.001.

[15] K. Scheufele, M. Mehl, Robust multisection quasi-Newton variants for parallel fluid-structure simulations—and other multiphysics applications, *Siam Journal on Scientific Computing* 39 (5) (2017) 404–433. doi:10.1137/16M1082020.

[16] T. Spenke, N. Hosters, M. Behr, A multi-vector interface quasi-Newton method with linear complexity for partitioned fluid–structure interaction, *Computer Methods in Applied Mechanics and Engineering* 361 (2020) 112810. doi:10.1016/j.cma.2019.112810.

[17] N. Delaissé, T. Demeester, D. Fauconnier, J. Degroote, Surrogate-based acceleration of quasi-Newton techniques for fluid-structure interaction simulations, *Computers & Structures* 260 (2022) 106720. doi:10.1016/j.compstruc.2021.106720.

[18] T. Demeester, E. H. van Brummelen, J. Degroote, An efficient quasi-Newton method for three-dimensional steady free surface flow, *International Journal for Numerical Methods in Fluids* 93 (8) (2021) 2581–2610. doi:10.1002/fld.4989.

[19] S. Badia, F. Nobile, C. Vergara, Fluid–structure partitioned procedures based on Robin transmission conditions, *Journal of Computational Physics* 227 (14) (2008) 7027–7051. doi:10.1016/j.jcp.2008.04.006.

[20] F. Nobile, C. Vergara, An effective fluid-structure interaction formulation for vascular dynamics by generalized Robin conditions, *Siam Journal on Scientific Computing* 30 (2) (2008) 731–763. doi:10.1137/060678439.

[21] L. Gerardo-Giorda, F. Nobile, C. Vergara, Analysis and optimization of Robin–Robin partitioned procedures in fluid-structure interaction problems, *Siam Journal on Numerical Analysis* 48 (6) (2010) 2091–2116. doi:10.1137/09076605X.

[22] S. Cao, A. Main, K. G. Wang, Robin–Neumann transmission conditions for fluid-structure coupling: Embedded boundary implementation and parameter analysis, *International Journal for Numerical Methods in Engineering* 115 (5) (2018) 578–603. doi:10.1002/nme.5817.

[23] S. Cao, G. Wang, K. G. Wang, A spatially varying Robin interface condition for fluid-structure coupled simulations, *International Journal for Numerical Methods in Engineering* 122 (19) (2021) 5176–5203. doi:10.1002/nme.6386.

[24] G. Gigante, C. Vergara, On the choice of interface parameters in Robin–Robin loosely coupled schemes for fluid–structure interaction, *Fluids* 6 (6) (2021) 213. doi:10.3390/fluids6060213.

[25] J. Degroote, On the similarity between Dirichlet–Neumann with interface artificial compressibility and Robin–Neumann schemes for the solution of fluid-structure interaction problems, *Journal of Computational Physics* 230 (17) (2011) 6399–6403. doi:10.1016/j.jcp.2011.05.012.

[26] J. Degroote, A. Swillens, P. Bruggeman, R. Haelterman, P. Segers, J. Vierendeels, Simulation of fluid-structure interaction with the interface artificial compressibility method, *International Journal for Numerical Methods in Biomedical Engineering* 26 (3-4) (2010) 276–289. doi:10.1002/cnm.1276.

[27] N. Hosters, Spline-based methods for fluid-structure interaction, Ph.D. thesis, RWTH Aachen University (2018). doi:10.18154/RWTH-2018-223770.

[28] L. Pauli, M. Behr, On stabilized space-time FEM for anisotropic meshes: Incompressible Navier-Stokes equations and applications to blood flow in medical devices, *International Journal for Numerical Methods in Fluids* 85 (3) (2017) 189–209. doi:10.1002/fld.4378.

[29] J. Donea, A. Huerta, *Finite Element Methods for Flow Problems*, John Wiley & Sons, 2003. doi:10.1002/0470013826.

[30] D. Forti, L. Dedè, Semi-implicit BDF time discretization of the Navier–Stokes equations with VMS-LES modeling in a high performance computing framework, *Computers & Fluids* 117 (2015) 168–182. doi:10.1016/j.compfluid.2015.05.011.

[31] A. A. Johnson, T. E. Tezduyar, Mesh update strategies in parallel finite element computations of flow problems with moving boundaries and interfaces, *Computer Methods in Applied Mechanics and Engineering* 119 (1-2) (1994) 73–94. doi:10.1016/0045-7825(94)00077-8.

[32] M. Behr, F. Abraham, Free-surface flow simulations in the presence of inclined walls, *Computer Methods in Applied Mechanics and Engineering* 191 (47-48) (2002) 5467–5483. doi:10.1016/S0045-7825(02)00444-9.

[33] C. Förster, W. A. Wall, E. Ramm, On the geometric conservation law in transient flow calculations on deforming domains, *International Journal for Numerical Methods in Fluids* 50 (12) (2006) 1369–1379. doi:10.1002/fld.1093.

[34] K.-J. Bathe, *Finite Element Procedures*, Klaus-Jurgen Bathe, 2006.

[35] T. J. Hughes, J. A. Cottrell, Y. Bazilevs, Isogeometric analysis: CAD, finite elements, NURBS, exact geometry and mesh refinement, *Computer Methods in Applied Mechanics and Engineering* 194 (39-41) (2005) 4135–4195. doi:10.1016/j.cma.2004.10.008.

[36] J. A. Cottrell, T. J. Hughes, Y. Bazilevs, *Isogeometric Analysis: Toward Integration of CAD and FEA*, John Wiley & Sons, 2009. doi:10.1002/9780470749081.ch7.

[37] J. Chung, G. Hulbert, A time integration algorithm for structural dynamics with improved numerical dissipation: The generalized- $\alpha$  method, *Journal of Applied Mechanics* 60 (1993) 371. doi:10.1115/1.2900803.

[38] S. Erlicher, L. Bonaventura, O. S. Bursi, The analysis of the generalized- $\alpha$  method for non-linear dynamic problems, *Computational Mechanics* 28 (2) (2002) 83–104. doi:10.1007/s00466-001-0273-z.

[39] M. K. P. Make, Spline-based methods for aerothermoelastic problems, Ph.D. thesis, RWTH Aachen University (2021). doi:10.18154/RWTH-2021-03363.

[40] N. Hosters, J. Helmig, A. Stavrev, M. Behr, S. Elgeti, Fluid–structure interaction with NURBS-based coupling, *Computer Methods in Applied Mechanics and Engineering* 332 (2018) 520–539. doi:10.1016/j.cma.2018.01.003.

[41] U. Küttler, W. A. Wall, Fixed-point fluid-structure interaction solvers with dynamic relaxation, *Computational Mechanics* 43 (1) (2008) 61–72. doi:10.1007/s00466-008-0255-5.

[42] T. Spenke, N. Hosters, M. Behr, The performance impact of the Newton iterations per solver call in partitioned fluid-structure interaction, in: 9th Edition of the International Conference on Computational Methods for Coupled Problems in Science and Engineering, 2021. doi:10.23967/coupled.2021.044.

- [43] B. M. Irons, R. C. Tuck, A version of the Aitken accelerator for computer iteration, *International Journal for Numerical Methods in Engineering* 1 (3) (1969) 275–277. doi:10.1002/nme.1620010306.
- [44] N. Delaissé, T. Demeester, D. Fauconnier, J. Degroote, Comparison of different quasi-Newton techniques for coupling of black box solvers, in: 14th World Congress on Computational Mechanics/8th European Congress on Computational Methods in Applied Sciences and Engineering, 2021. doi:10.23967/wccm-eccomas.2020.088.
- [45] W. Dornisch, S. Klinkel, B. Simeon, Isogeometric Reissner–Mindlin shell analysis with exactly calculated director vectors, *Computer Methods in Applied Mechanics and Engineering* 253 (2013) 491–504. doi:10.1016/j.cma.2012.09.010.